Breakdown Anodization (BDA) for Hierarchical Structures of Titanium Oxide

by

Soon Ju Choi

B.S., Seoul National University (2010)

Submitted to the Department of Mechanical Engineering
in partial fulfillment of the requirements for the degree of

Master of Science in Mechanical Engineering

at the

MASSACHUSETTS INSTITUTE OF TECHNOLOGY

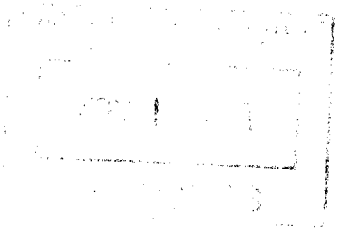

August 2013
[SEPTEMBER 2013]

Author .....
Department of Mechanical Engineering
August 23, 2013

Certified by .....
Cullen R. Buie
Assistant Professor
Thesis Supervisor

Accepted by .....
David E. Hardt
Graduate Officer, Department of Mechanical Engineering

Breakdown Anodization (BDA) for Hierarchical Structures of Titanium Oxide

by

Soon Ju Choi

Submitted to the Department of Mechanical Engineering
on Aug 16, 2013, in partial fulfillment of the
requirements for the degree of
Master of Science in Mechanical Engineering

Abstract

Breakdown Anodization (BDA) of titanium dioxide is a very promising, fast fabrication method to construct micro-scale and nano-scale structures on titanium surfaces. This method uses environmentally friendly electrolytes, such as nitric acid, and can be fabricated within 30 minutes regardless of substrate size. Because the titanium dioxide is hydrophilic, the micro structured BDA surface exhibits super-hydrophilic properties. BDA surfaces can be applicable to water transport, chromatography, electrospray, and fabrication of hierarchically structured surfaces. In this study we investigate the wicking properties of BDA surfaces and quantify their performance in terms of capillary pressure and capillary spreading speed constant. Further, we investigate the application of BDA surfaces to electrospray for the separation and identification of chemical agents.

Thesis Supervisor: Cullen R. Buie
Title: Assistant Professor

Acknowledgements

I would like to thank my advisor, Professor Cullen Buie, for his guidance and support throughout my master's program. I have learned a great deal from him, especially in developing my career path as an engineer.

I would also like to thank my colleagues, Youngsoo Joung, Zhife Ge, Qianru Wang, William Braff, Bruno Figliuzzi, Alisha Schor, Naga Neehar Dingari, Andrew Jones, and Pei Zhang, at Laboratory for Energy and Microsystems Innovations. They have provided me with invaluable advice and encouragement. I want to send my special appreciation to Youngsoo Joung who has given me great insight into my research with his experiences and wisdom.

I also want to send thanks to Professor Sang-gook Kim and Rohit Karnik for giving me opportunity to work in such a great environment, and Dr. Jim Bales in Edgerton Center who provided me the high speed camera for my research. I am also indebted to Byung Gu Cho, Kyoo-Chul Park and friends for their support and kind words.

Lastly, I want to send my appreciation to Chong-Hwan Lee, the founder of Kwanjeong Foundation, for supporting me and believing in my possibilities. He has been my mentor, cheering me through the ups and downs.

And above all, my warmest regard and deepest love goes to my family in Korea.

Contents

List of Figures

List of Tables

Chapter 1

Introduction

1.1 Motivation of the Research

Titanium dioxide is a promising material, which can be applied to various applications with various fabrication methods. Applications include photocatalysis [1], catalysis [2], solar cells [3], and biomedical devices [4]. When the titanium is anodized, its surface can be modified to various structures with special properties according to electrolyte condition and applied voltage.

Breakdown anodization is an anodization method using titanium substrate [6], which is able to rapidly fabricate microstructures using an environmentally friendly electrolyte, nitric acid.

1.2 Goal of the Research

Tianium dioxide is high surface energy and BDA surface is conductive material having various applications. First, it is important to determine how experimental conditions including electrolyte temperature and applied voltage affect the surface properties. This would enable the fabrication of BDA surfaces with specific, deterministic properties by adjusting the experimental conditions.

Through this study, BDA surfaces are applied to electrospray and this work also explores fabrication of hierarchical titanium surfaces by coupling BDA with other etching processes.

Chapter 2

Research Background

2.1 Capillary Flow

BDA surfaces are hydrophilic, the wetting line rises to certain height when it contact the water reservoir. The hydrophilic BDA surface can be modeled as columns of capillaries and the wetting behavior can be approximated by Washburn's equation [5].

$$\frac{dh}{dt} = \frac{r^2}{8\eta h}\left[\frac{2\gamma\cos\theta}{r} - \rho g h\right] \tag{2.1}$$

Where h is the vertical height of the liquid; t is the elapsed time after liquid contact; r is the assumed pore radius; γ is the liquid surface tension; ρ is the liquid density; η, θ, and g are the liquid viscosity, surface native contact angle, and gravitational

constant, respectively. At the initial stage, the gravity term is negligible and equation (2.1) becomes [6],

$$h^2 = \frac{r\gamma \cos\theta}{2\eta} t = \frac{1}{2} C_{cap} t \tag{2.2}$$

Where C_{cap} is called the spreading speed constant. From the initial elapsed time of capillary rise experiment, the curve for liquid height according to time can be obtained to find the spreading speed constant by curve fitting.

Capillary pressure can be calculated when the liquid reachs the maximum rise height. At this location the gravitational force balances the capillary force, assuming negligible liquid evaporation. Then the time term of equation (2.1) is neglected and balances the rest terms and becomes [6],

$$P_{cap} = \frac{2\gamma \cos\theta}{r} = H_{max} g \rho \tag{2.3}$$

Where H_{max} indicates the maximum capillary height.

2.2 Anodization Process

The anodization process forms a thin oxide layers on the positive electrode [7]. Traditional titanium anodization forms thin and compact titanium dioxide layers. One of example conditions for this thin compact layers is anodization in pH.1.0 H_3PO_4 electrolyte with 100V/cm applied voltage [8].

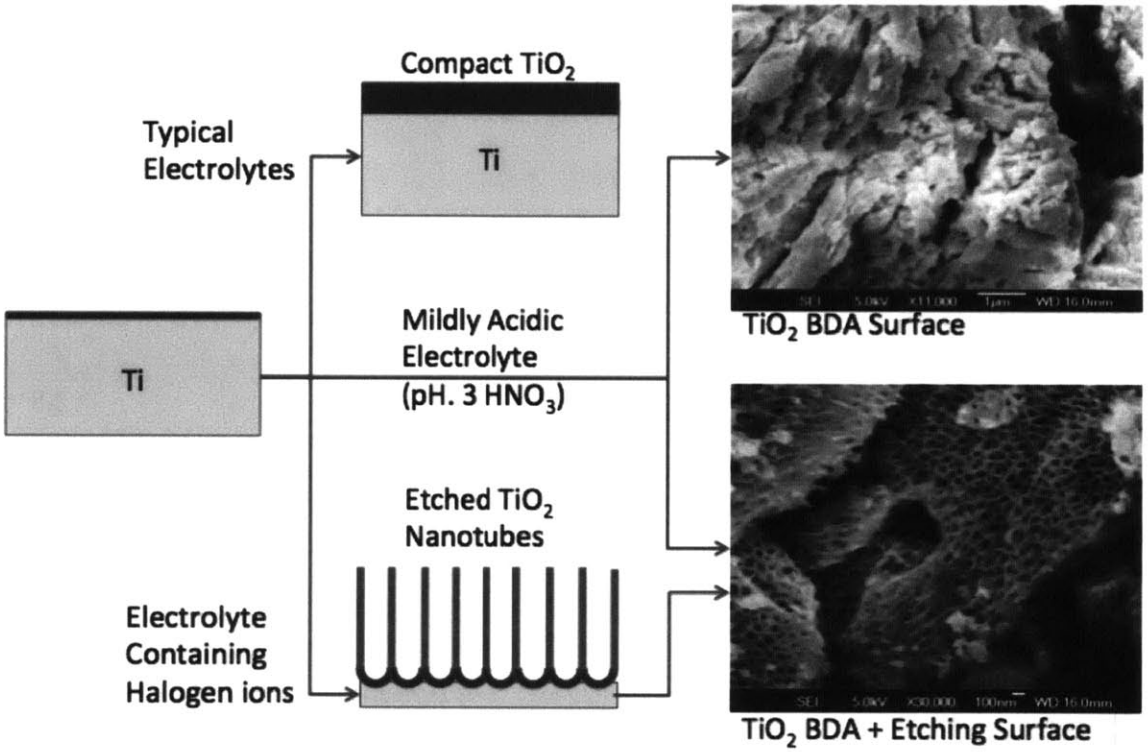

Figure 2-1: Anodization, breakdown anodization (BDA), and etching according to electrolyte conditions.

Also instead of using titanium, other materials such as Zr [9], Ta [10], and W [11] can be used to form oxide films. The anodic film formation on the titanium surface is governed by following reaction [6],

<Anode>

Electrolysis:

$$2H_2O \rightarrow O_2(g) + 4H^+ + 4e^- \quad (2.4)$$

Corrosion:

$$Ti \rightarrow Ti^{3+} + e^- \quad (2.5)$$

Oxidation:

$$Ti + 2H_2O(l) \rightarrow TiO_2 + 4H^+ + 4e^- \quad (2.6)$$

$$Ti + O^2 \rightarrow TiO_2 \quad (2.7)$$

Dissolution:

$$TiO_{2-x} + H_2O(l) \rightarrow TiO_{2-x}H_2O(s) \quad (2.8)$$

$$TiO_2 + H_2O + H^+ \rightarrow Ti(OH)_3 \quad (2.9)$$

<Cathode>

Electrolysis:

$$4H_2O + 4e^- \rightarrow 2H_2(g) + 4OH \quad (2.10)$$

Electrodeposition:

$$Ti^{3+} + 3e^- \rightarrow Ti \quad (2.11)$$

Electrolysis (2.10) and dissolution (2.8), (2.9) are continuous processes during anodization. Corrosion and electrodeposition terminate at the initial state because the formed oxide layer prevents the both reactions. At steady state, therefore, electrolysis, oxidation, and dissolution mainly occur yielding the overall reaction,

$$0.5\ Ti + 2H_2O\ (l) \rightarrow 0.5\ TiO_2 + 2H_2\ (g) + 0.5\ O_2\ (g) \tag{2.12}$$

2.2.1 Breakdown Potential

The breakdown of the oxide layer was theoretically well explained by the paper of Sato in 1971 [12]. The surface pressure during the anodization process can be explained by main two forces, an electrostriction effect and the interfacial tension effect as follows;

$$P = P_0 + \frac{\varepsilon(\varepsilon - 1)E^2}{8\pi} - \frac{\gamma_e}{L} \tag{2.13}$$

with the vertically acting pressure P; the atmospheric pressure P_0; electric field E; dielectric constant of the film ε; γ_e surface tension of the oxide film; and oxide film thickness L.

When the surface tension has a major effect on the surface, the electrochemical property of electrolyte and electrodes must be considered to

predict the breakdown conditions because ion adsorption of the film surface affects the surface tension. The break down electric field, E_c on the oxide layer can be expressed as follows [6];

$$E_c = \frac{\phi - \phi_f}{L} \tag{2.14}$$

where electrode potential ϕ; and equilibrium potential between the oxide layer and the electrolyte ϕ_f; and thickness L. After breakdown occurs, the electrode potential ϕ^*, can be expressed by [12]

$$\frac{d\phi^*}{dlna} = -\frac{8\pi k_B T \rho_a}{8\pi\sigma_0 - \varepsilon(\varepsilon+1)E_c} \tag{2.15}$$

where the activity of anion in the electrolyte is a; and absorption density of anions is ρ_a. At higher temperature conditions, critical potential will be lowered.

2.2.2 Breakdown Anodization (BDA) Process

Breakdown occurs when the electric potential exceeding the breakdown potential and forms the micro structures on the electrode. This phenomenon is typically

observed over 60 V when pH 3 nitric acid was used for the process. The process forms micro sized structures on the surface, increasing it's roughness. Because the static contact angle of titanium dioxide with water is below 90°, BDA surfaces are hydrophilic. This surface, therefore, is ideal for highly absorbent applications such as extracting fluids from soil in which high absorbency is necessary.

2.2.3 Temperature of BDA process

The oxide layer thickness of the BDA process is mainly governed by the electrolyte temperature and applied electric potential for a given electrolyte. The dissolution rate is the hydration process of titanium dioxide layer, which governs the oxide film thickness. Electrolyte temperature largely affects the hydration rate; therefore, temperature of the electrolyte controls the oxide film thickness [56].

The oxide layer thickness can be measured using the surface capacitance because the oxide layer thickness is inversely proportional to the capacitance of the oxide layer, $1/C_f$ [13]. A relation suggested by Bockris et al. [14] is as follows,

$$\left[\frac{dln(C_f^{-1})}{dt}\right]_{C_f^{-1}} = -\frac{\Delta H}{RT} \tag{2.16}$$

with time, t; universal gas constant, R; and activation energy, ΔH.

2.3.4 Etching Process

Etching process is mostly governed by chemical dissolution of the oxide layer by the presence of halogen ions in the electrolyte. The most common chemical material used for this process is hydrogen fluoride. The reaction converting the oxide layer to the soluble fluoride complex is as follows [7],

$$MeO_2 + 6F^- \rightarrow [MeF_6] \quad (2.17)$$

$$Me^{4+} + 6F^- \rightarrow [MeF_6]^{2-} \quad (2.18)$$

This process transforms the oxide layer, MeO_2, to water soluble MeF_6 complexes. The small radius vacancy made by dissolved oxide initiates the process. The complex formation continuously dissolves MeO_2 and prevents $Me(OH)_xO_y$ precipitation by transforming the arriving Me^{4+} ions at the oxide/solution interface to soluble MeF_6 complexes.

2.3 Soil Matric Potential

Unsaturated soil is a porous media which readily absorbs liquids. Soil science characterizes the medium by the matric potential or matric suction with respect to

the soil water content. The required energy to remove water held between the soil pores is matric potential. Matric suction is the same absolute value but the opposite sign as the matric potential. Normalized water content or effective saturation of the soil can be related by following expression [15],

$$S = \Theta = \frac{\theta - \theta_r}{\theta_s - \theta_r} = \left[\frac{1}{1 + (\alpha\psi)^n}\right]^m \tag{2.19}$$

where,

S, Θ are effective saturation, and normalized water content;

ψ is matric potential;

θ ,θ_s, and θ_r are volumetric water content, saturated water content, and residual water content, respectively;

$\alpha, n,$ *and* m are parameters relate to soil properties.

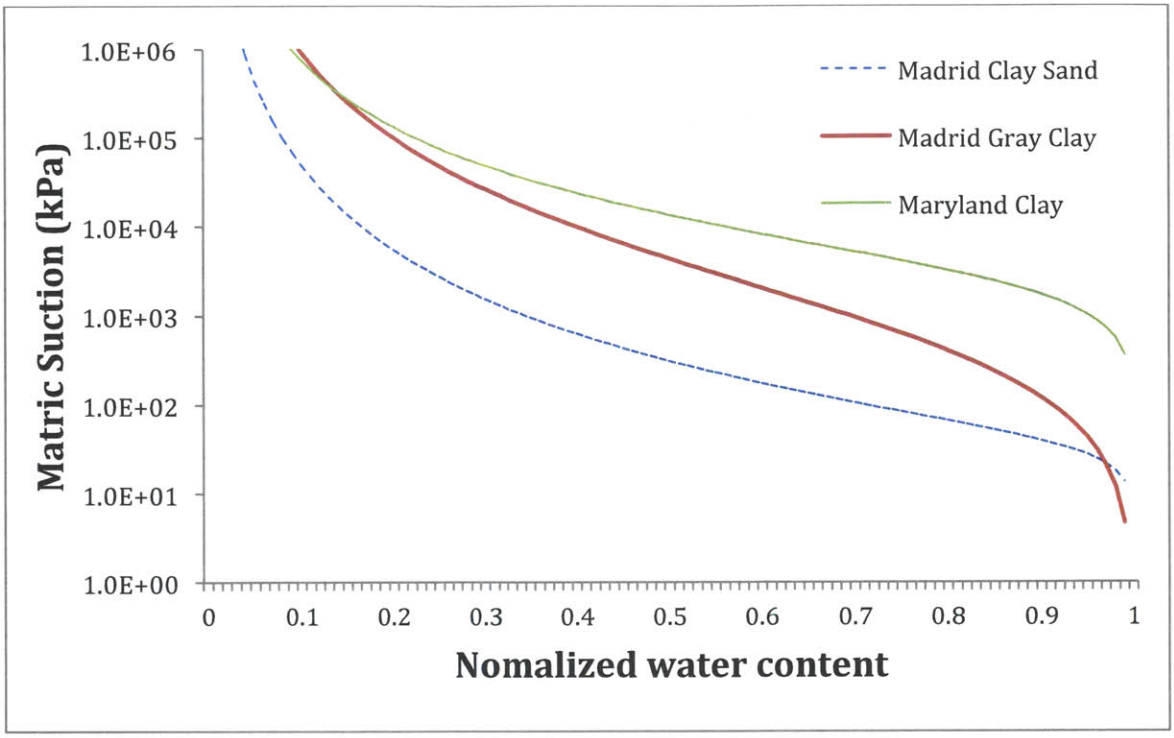

Figure 2-2: Graph for Water content and Matric suction based on the van Genuchten Model from equation 2.19, data is from Shada H. Krishnapillai, [16].

Table 2-1: Soil data is from Shada H. Krishnapillai [16]. Parameters a, n, and m is properties of soil for equation 2.19.

Soil Type	Porosity	Liquid Limit	a	n	m
Madrid clay sand	0.275	28%	0.028	2.55	0.125
Madrid gray clay	0.507	71%	0.0015	0.75	0.425
Maryland clay	0.448	64%	0.0004	1.65	0.245

As shown above, the matric suction decreases as the water content increases. Also when the water content is the same, the small pore size soil or clay

has larger matric suction values than that of larger sized soil (e.g. sand). It means that the retained water between the small pores requires more energy to extract than larger pore size soil when it has identical water content.

2.4 Electrospray

Traditional electrospray uses stainless capillary tips (diameter about 1mm) to form gas phase ions. Depending upon whether it is connected to the positive electrode or negative electrode, the spray is denoted positive mode or negative mode. Most electrospray applications use the positive mode, which makes positive ions. The electric field at the tip is calculated by following equation (Loeb et al., 1941, [17]).

$$E_c = \frac{2V_c}{R \ln (4d/R)} \tag{2.20}$$

with the electric field, E_c; the applied potential, V_c; distance from the tip and the counter electrode, d; and the capillary outer diameter, R. It means that the electric field is proportional to the applied voltage and inversely proportional to the distance from the tip and the counter electrode, and the capillary outer diameter.

As the applied voltage increases, the electric field also increases and the solution at the tip eventually becomes the Taylor cone shape when it starts electrospray. The positive ions mostly located at the surface of Taylor cone spray positive ion-rich droplets to the counter electrode. As soon as the positive ion rich droplet leaves the tip to the counter electrode, the solvent of the solution (usually methanol) evaporates until ions become gas phase due to the repulsive force between the ions.

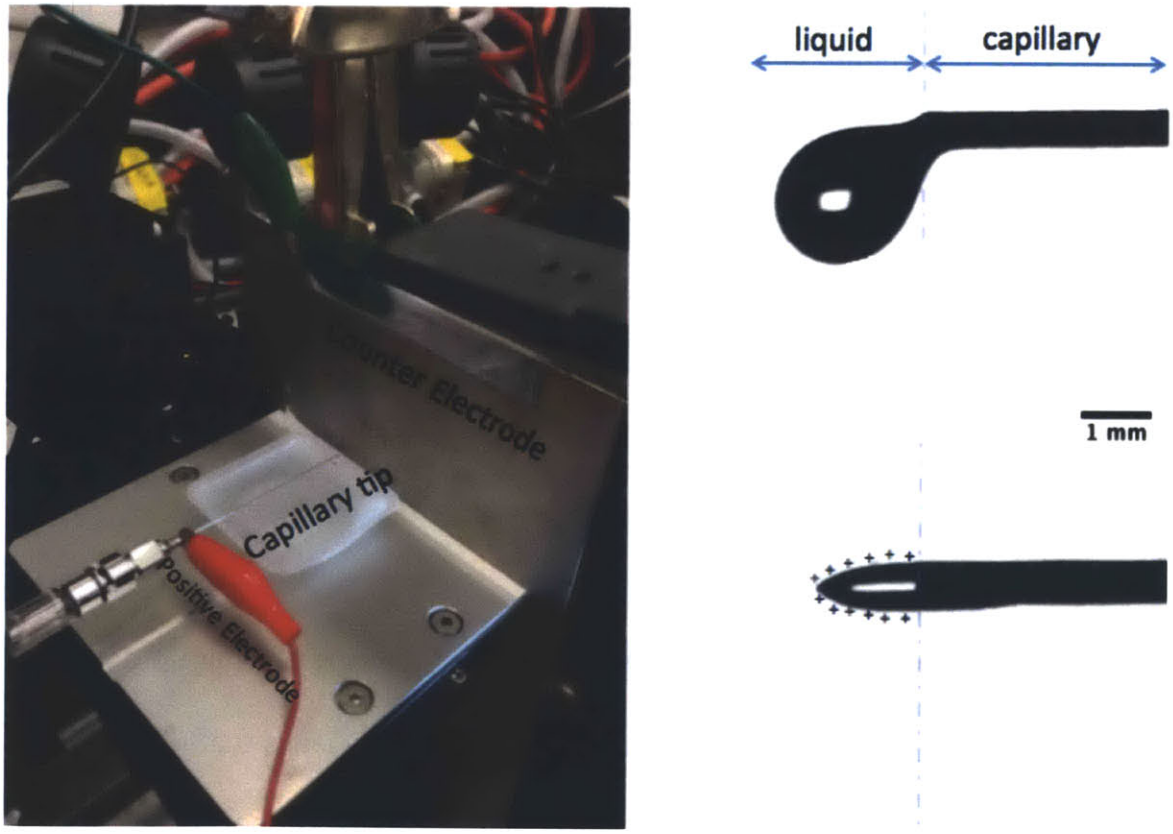

Figure 2-3: Apparatus for traditional capillary tip electrospray (left), and spray formation (right). Spray occurs and a Taylor cone is formed at 4.0 kV. The solution surface is positively charged due to the electric field.

Instead of using tubular capillaries, stainless steel needles [18, 25], tungsten oxide nanowire[19], wooden toothpicks [20], or even paper [21-24] have been used as electrospray tips. Although these tip are not conductive, electrospray occurs because the applied solution was conductive. These tips are able to make small diameter electrosprays compared to traditional capillaries. The advantage is that these systems can utilize smaller sample volumes than traditional capillaries.

Chapter 3

Fabrication Method

3.1 Breakdown Anodization (BDA)

The cathode and anode for the BDA process were prepared from the titanium plates (Ultra Corrosion-Resistant Titanium grade 2, 0.02" thick). Their dimensions were 10 mm x 170 mm. To eliminate contaminants on the titanium electrodes, each sample was cleaned with acetone, methanol, isopropanol, and DI water. The cathode and anode were assembled maintaining a 10 mm distance by inserting non-conducting material between the electrodes.

Four electrodes were immersed into acetic acid at pH 3 and a constant voltage (range 30V-120V) was applied for 30 minutes. Using a circulation bath (polystat, Cole-Parmer), the temperature during the process was held constant (range 10°C - 25°C). Stirrer with 800rpm was used to circulate the electrolyte to eliminate the by-products on electrodes. After the entire process the BDA surfaces were cleaned with DI water.

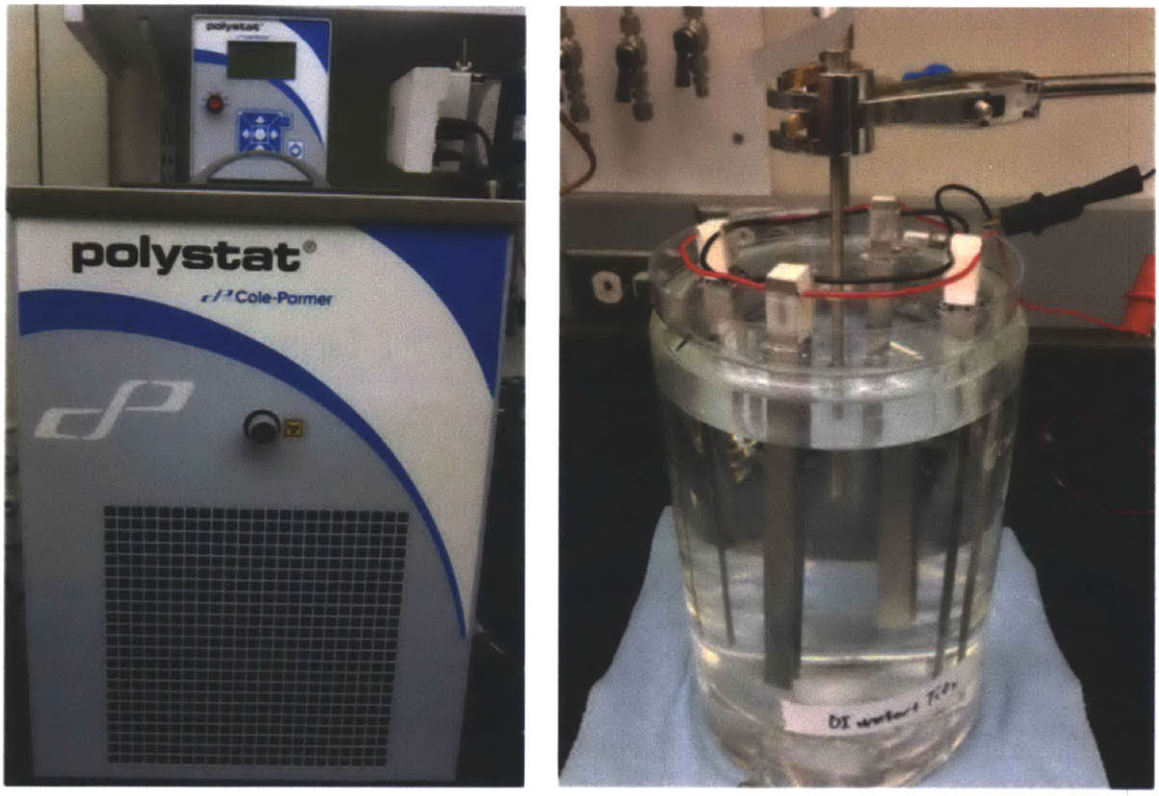

Figure 3-1: Circulation bath for control temperature (left), and BDA apparatus with thermal couple to measure the electrolyte temperature (right).

The temperature of the circulating liquid was maintained five degrees below the target temperature to account for heat generation during BDA. The circulating liquid maintains the electrolyte temperature by removing the heat produced due to BDA.

A more direct way to control the electrolyte temperature is to use the electrolyte as the circulating fluid. In this case the electrolyte temperature is set directly by the water bath, eliminating the need for stirring or a thermocouple.

3.2 Capillary Rise Experiments

Capillary rise experiments are utilized to measure the capillary pressure and spreading speed constant of the BDA surface. The microstructure of the BDA surface depends on the fabrication conditions- including electrolyte temperature, electrolyte pH, and applied voltage. As a result, the spreading speed and rise height on the BDA surface change under different fabrication conditions.

The capillary rise experiment consists of the following steps. First, the BDA surface is placed in the water reservoir. Then, the stage is adjusted such that the liquid comes into contact with the BDA surface. Spreading speed constant is calculated within the first five minutes. After 30 minutes, a photo is taken to determine the maximum capillary rise height.

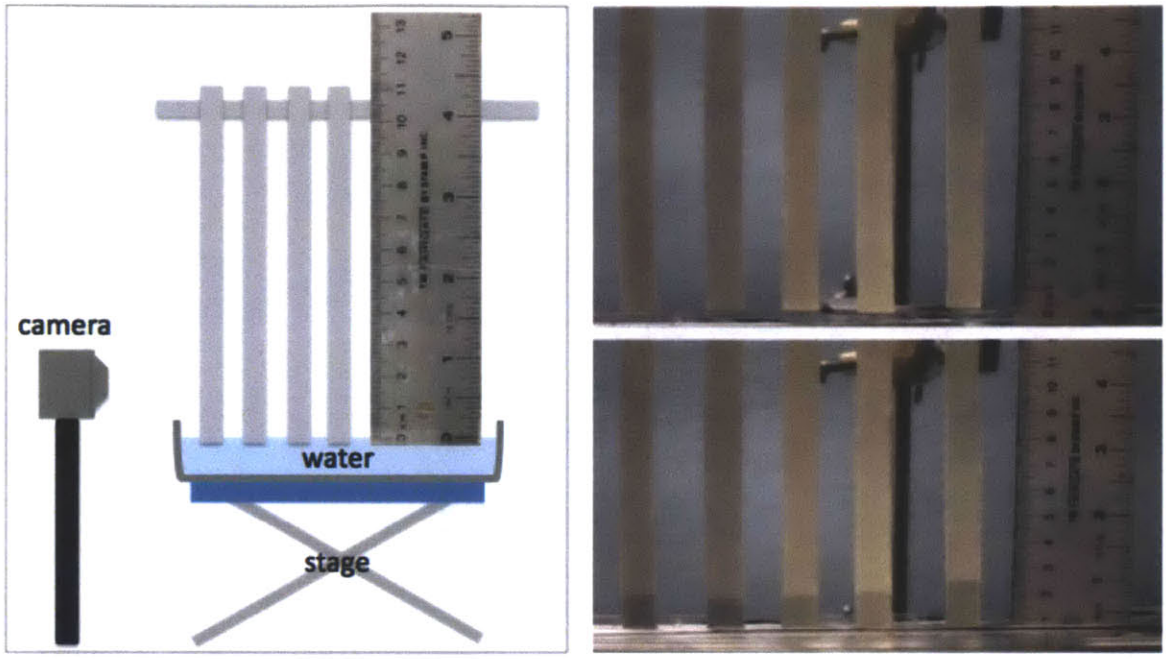

Figure 3-2: Capillary rise experiment (left), and image of the experiment before and after 0.5 seconds the sample is emerged water (right).

3.3 Electrospray

As discussed in section 2.4, the electrospray performance depends on the electric field at the edge of the capillary or tip. Therefore, it is important to sharpen the BDA tip to maximize the electric field and lower the required applied voltage. In general, the sharp edge showed better performance compared to the planar edge.

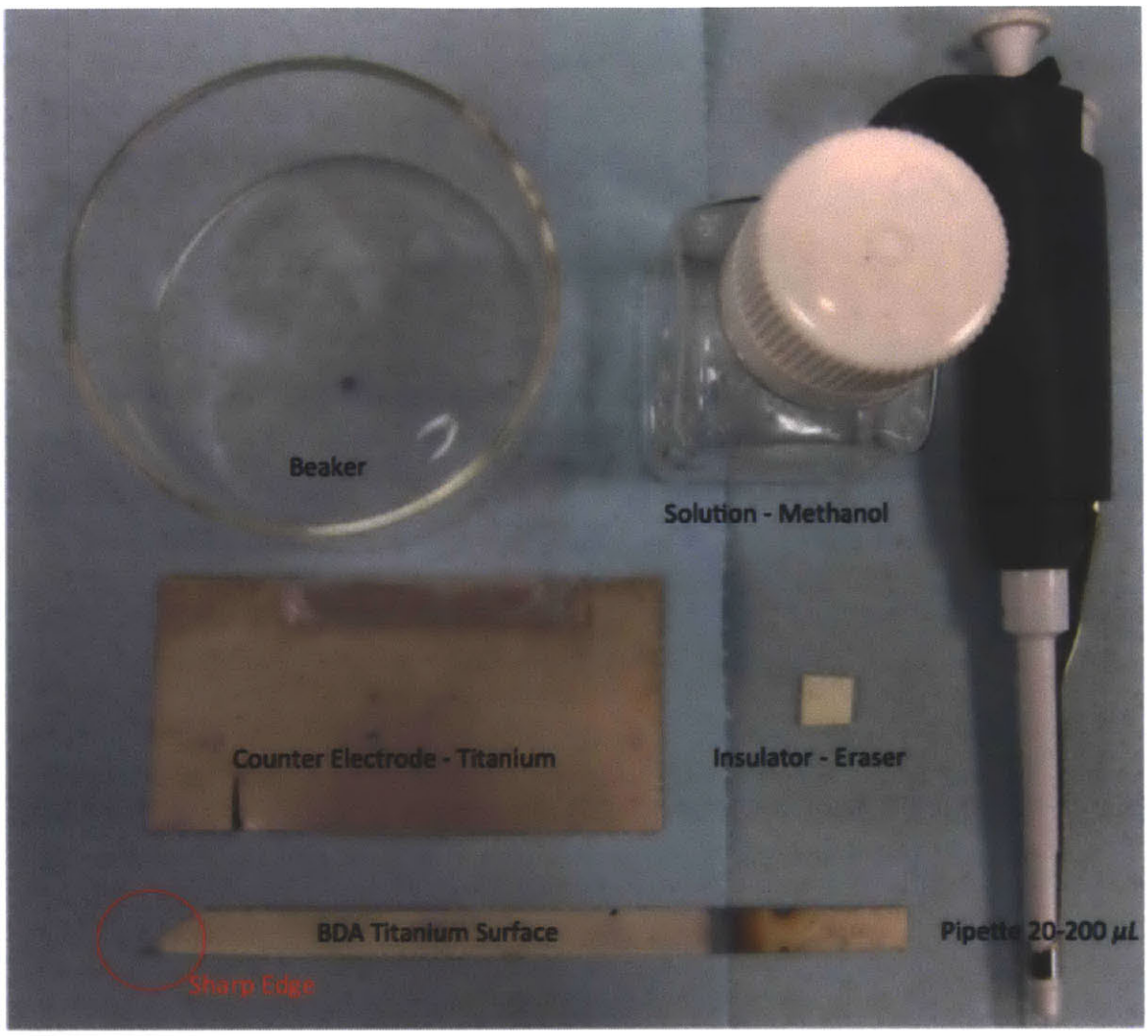

Figure 3-3: Experimental materials and equipment for electrospray.

Methanol was used as solvent due to its high evaporation rates. Chemicals were also added in solution to enhance the conductivity and for detection by mass spectrometry. The methanol solution was 1.5 wt% methanol with Methyl Blue, Fluorescein, and Rhodamine B fluorescent dyes. Due to its distinct color and different mobility on the BDA surface, it is straightforward to identify the chemicals with the naked eye during the experiment.

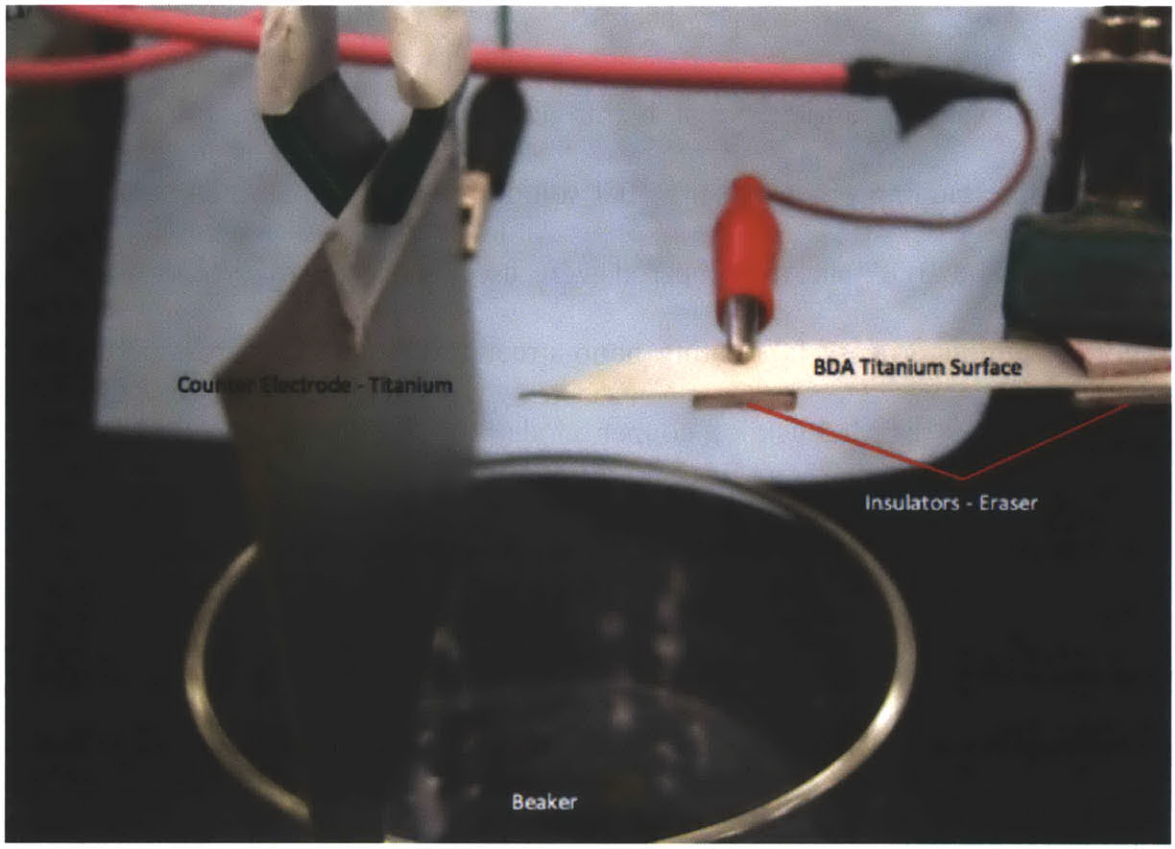

Figure 3-4: Electrospray was connected to a power supply and ready to spray.

As mentioned earlier, the distance between the counter electrode and the BDA surface was 10 mm. Also to focus electric field to the upper-side of the BDA surface which contained the liquid analyte, the bottom side of the BDA surface was electrically insulated from the electrode. After the solution placed onto the BDA surface, a 4.5 kV of electric potential was applied using a power supply. Immediately after the solution reached the BDA tip, it emitted small droplets to counter electrode.

3.4 Safe Etching Process

This section explores fabrication of hierarchical titanium surfaces by coupling BDA with safe etching process using HCl solution instead of using conventional HF solution. The BDA surface prepared were used as the positive electrode for additional etching process fabricating nano-structures on BDA micro-structures. Electrodes were assembled using a copper anode [26] as a counter electrode. This assembly was immersed into the 3M HCl while applying a constant potential of 10 V for 10 minutes. A stirrer was not used during this process and the surfaces were cleaned using DI water.

Figure 3-5: Etching Process (left), and capillary rise experiment of etched BDA surface. First sample from the right is etched BDA surface (right).

Chapter 4

Experiments, and Results

4.1 Wetting Properties

The capillary rise experiment measures two values; 1) P_{cap}: capillary pressure, and 2) C_{cap}: spreading speed constant. The result of the capillary rise experiment can be used to compare the wicking ability of the BDA surfaces to commercial materials such as thin layer chromatography (TLC) plates (Sigma-Aldrich, aluminum support, silica gel matrix, layer thickness 200 μ m, particle size 25 μ m). The experiments reveal that the BDA surfaces have higher capillary pressure and spreading speed constant than the commercial TLC plates.

The spreading speed constant and capillary pressure can be obtained using equations (2.2), and (2.3). From the equation (2.3), $P_{cap} = H_{max} g\rho$, capillary pressure is proportional to the maximum rise height.

In section 2.2.3, we verify that the applied voltage can affect the microstructure at the surface. To find the optimized voltage, we applied voltages of 30 V, 60 V, 90 V, and 120 V.

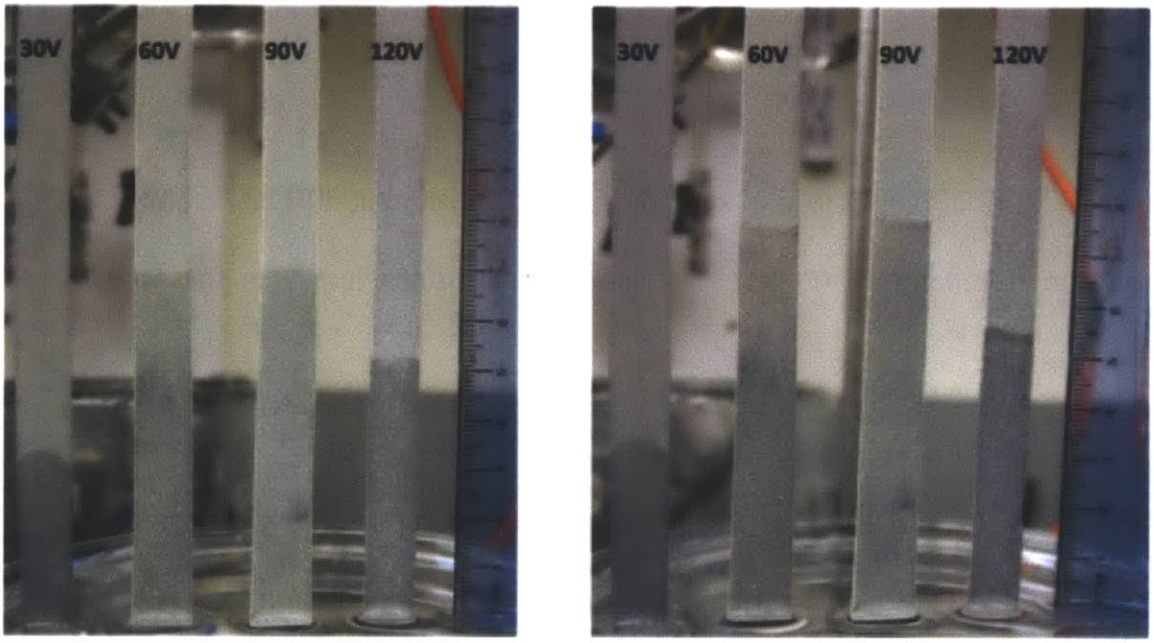

Figure 4-1: Constant temperature 20°C, left after 15 minutes, right after 30 minutes. Almost reached maximum capillary height after 15 minutes.

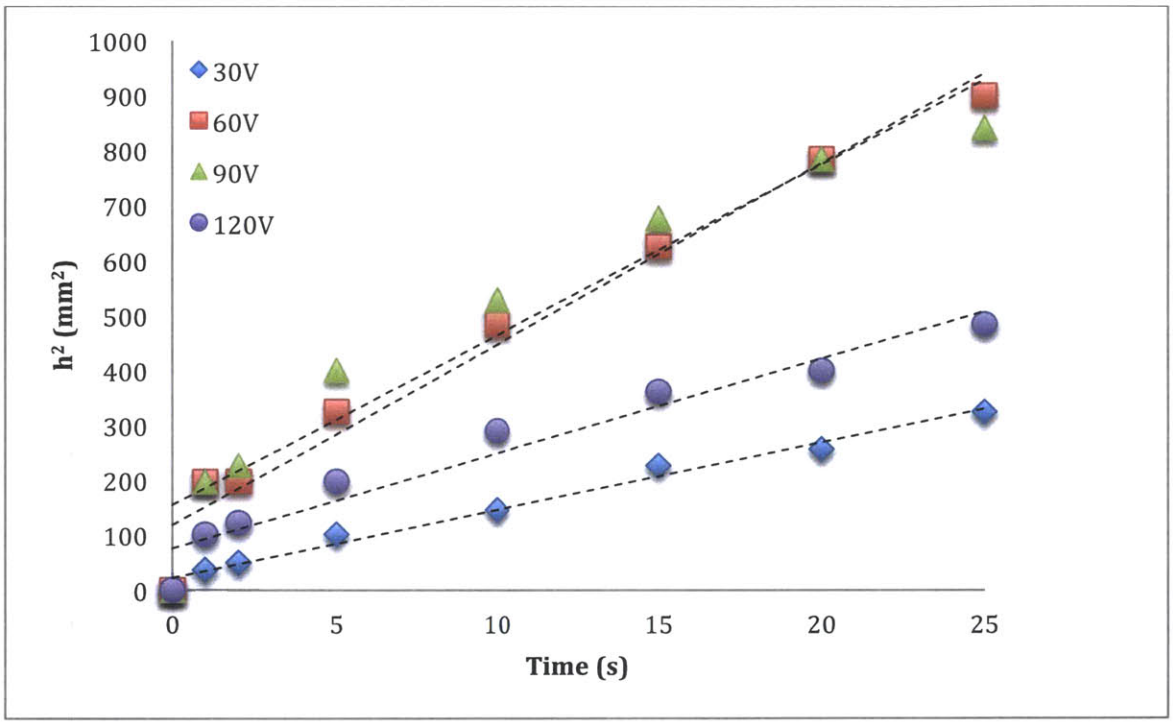

Figure 4-2: Initial height to find spreading speed constant at 30V, 60V, 90V, 120V at constant temperature (20°C). The slope of the lines indicates the spreading speed constant.

Table 4-1: Values of maximum capillary height (H_{max}), capillary pressure (P_{cap}), and spreading speed constant (C_{cap}) at constant electrolyte temperature (20°C) with respect to applied voltage.

	H_{max} (mm)	P_{cap} (kPa)	C_{cap} (mm²/s)
30V BDA	**35**	**0.35**	**12**
60V BDA	**80**	**0.81**	**30**
90V BDA	**80**	**0.81**	**33**
120V BDA	**55**	**0.56**	**17**

The best performance of capillary pressure and capillary spreading constant was found at 90 V with values of 0.81 kPa, and 33 mm^2/s for capillary pressure and capillary spreading constant, respectively.

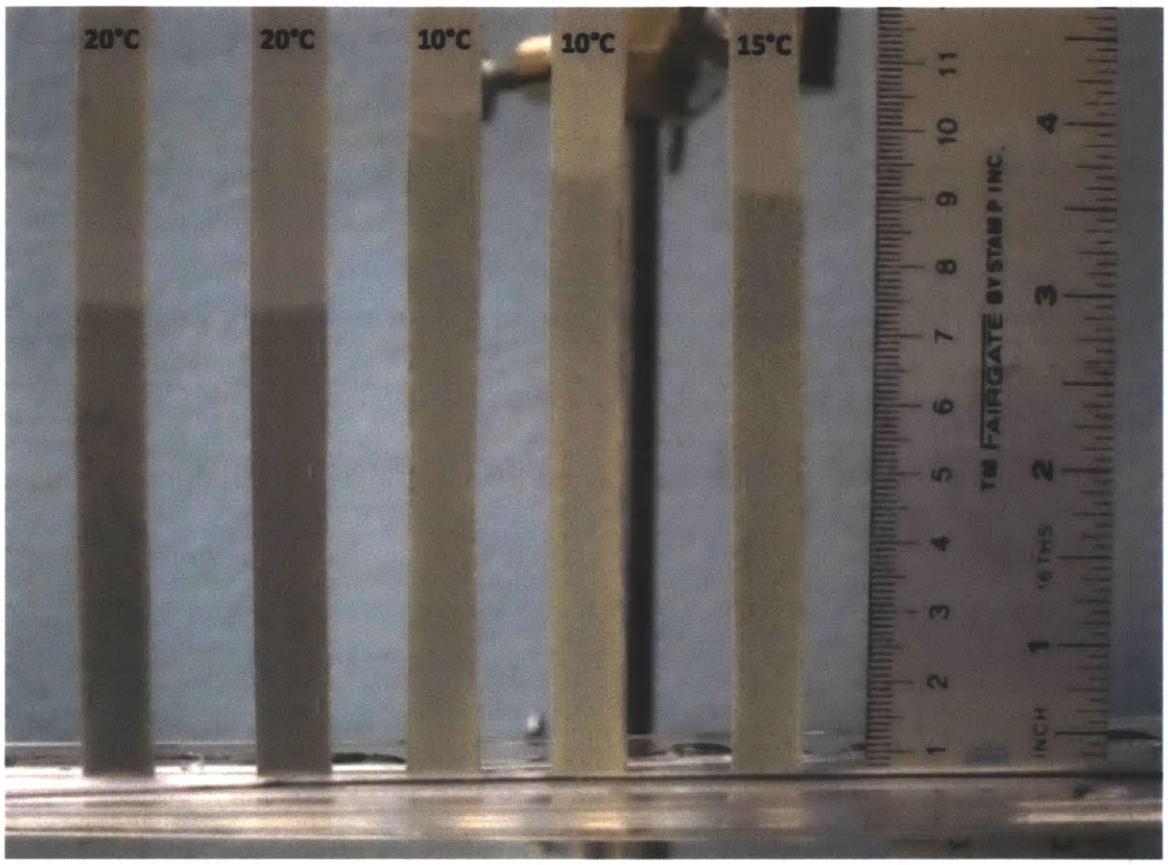

Figure 4-3: Constant Voltage 90V, and maximum capillary height. 30 minutes after immersed into the water.

Table 4-2: Values of maximum capillary height (H_{max}), capillary pressure (P_{cap}), and spreading speed constant (C_{cap}) at constant applied voltage (90V) with respect to electrolyte temperature.

	H_{max} (mm)	P_{cap} (kPa)	C_{cap} (mm^2/s)
10°C, 90V BDA	**100**	**1.1**	**55**
15°C, 90V BDA	**90**	**9.9**	**50**
20°C, 90V BDA	**75**	**0.83**	**41**

We also find that the temperature affects the microstructure of the BDA surface. Surfaces were fabricated at temperatures of 10°C, 15°C, and 20°C. The best performance was obtained at 90 V, and 20°C electrolyte temperature. At this condition, capillary pressure was 1.1kPa, and the capillary spreading constant was 55 mm^2/s.

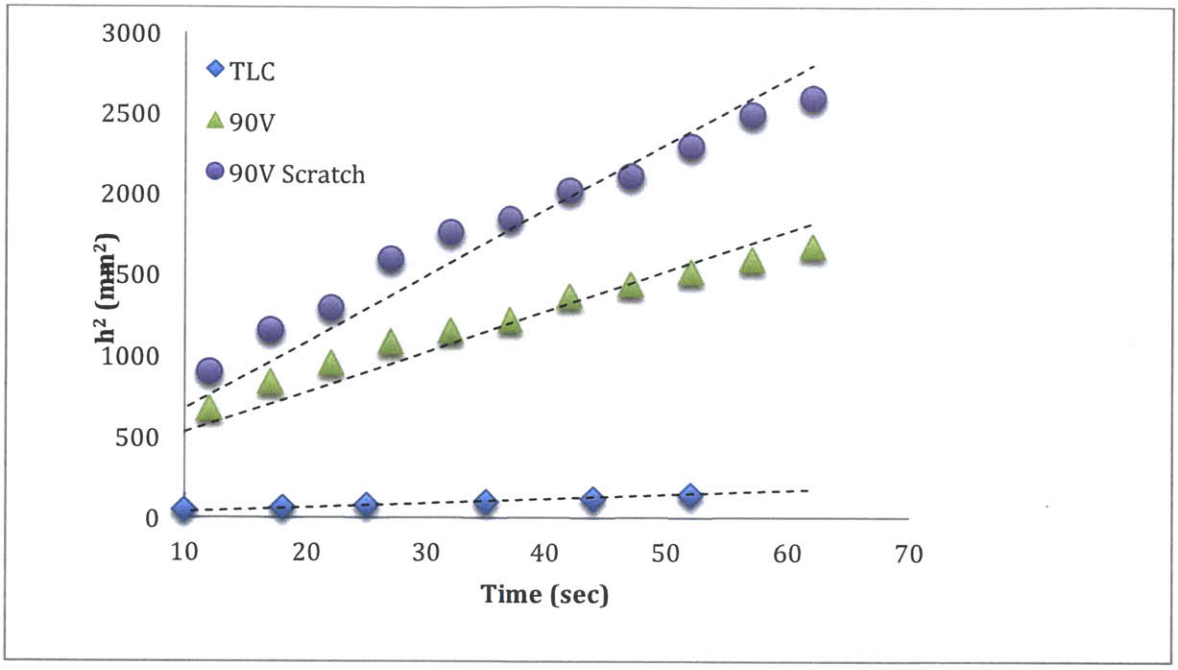

Figure 4-4: Initial height to find spreading speed constant of commercial TLC Plate, optimized condition (90V, 10 °C) BDA surface, and vertically scratched BDA surface. The slope of the lines indicates the spreading speed constant.

Table 4-3: Values of maximum capillary height (H_{max}), capillary pressure (P_{cap}), and spreading speed constant (C_{cap}) for commercial TLC Plate, optimized condition (90V, 10 °C) BDA surface, and vertically scratched BDA surface.

	H_{max} (mm)	P_{cap} (kPa)	C_{cap} (mm^2/s)
TLC	**40**	**0.40**	**3**
BDA 90V	**80**	**0.81**	**25**
BDA 90V Scratch	**85**	**0.86**	**41**

Moreover, the BDA surface is more resistive than the commercial TLC plate because the BDA surface is directly fabricated on the titanium metal substrate instead of being deposited on the substrate. Also from the capillary rise experiment with DI water, its capillary pressure was 0.8 kPa, compared to the capillary pressure of the commercial TLC of 0.4 kPa. The surface also showed faster spreading speed with a value of 25 mm^2/s, eight times faster than the TLC plate. Also, it was found that vertical scratches on the surface enhanced the capillary pressure and capillary speed. The capillary pressure increased by 125% for the 90 V BDA surface.

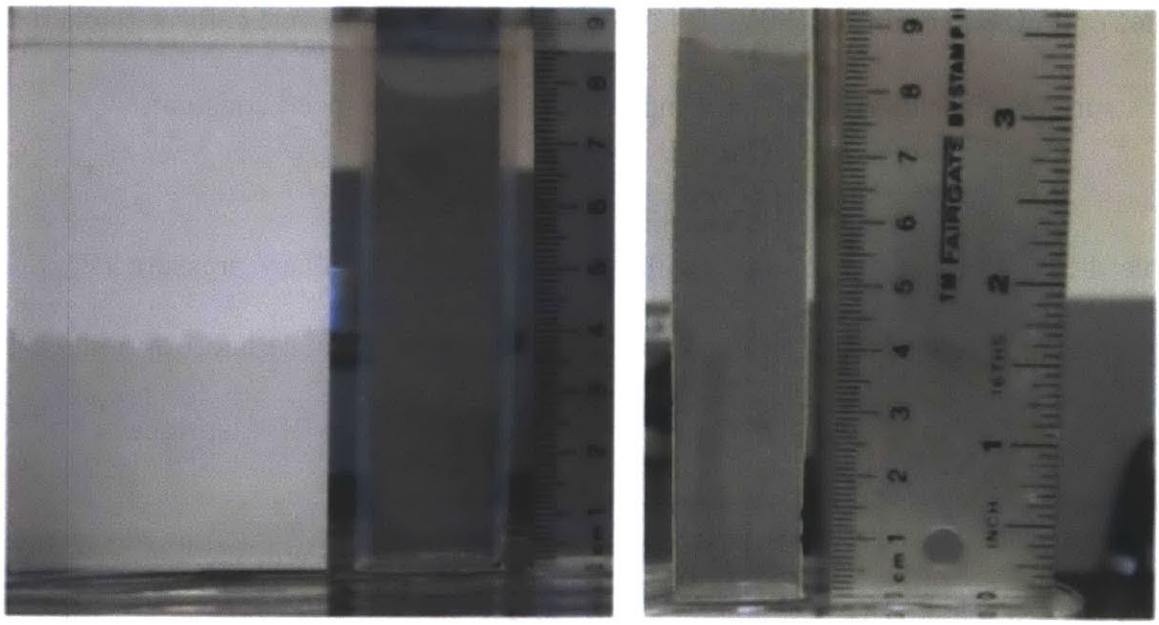

Figure 4-5: After 30 minute of capillary rise experiment for TLC, Optimized BDA surface, and scratched BDA surface.

4.2 Soil Experiment

Soil experimentation is required for the application of remote sensing as introduced in part 1. Titanium BDA surfaces are made from robust metal, making it ideal for use in soil wicking. In this experiment, the maximum volumetric liquid limit of soil was 31.9%.

When its water content increases the matric suction of the soil decreases as investigated at section 2.3 and finally can be ignored when it is saturated. Even when the water content was below (5 ml/35 ml) the BDA surface wicked the water 8 mm.

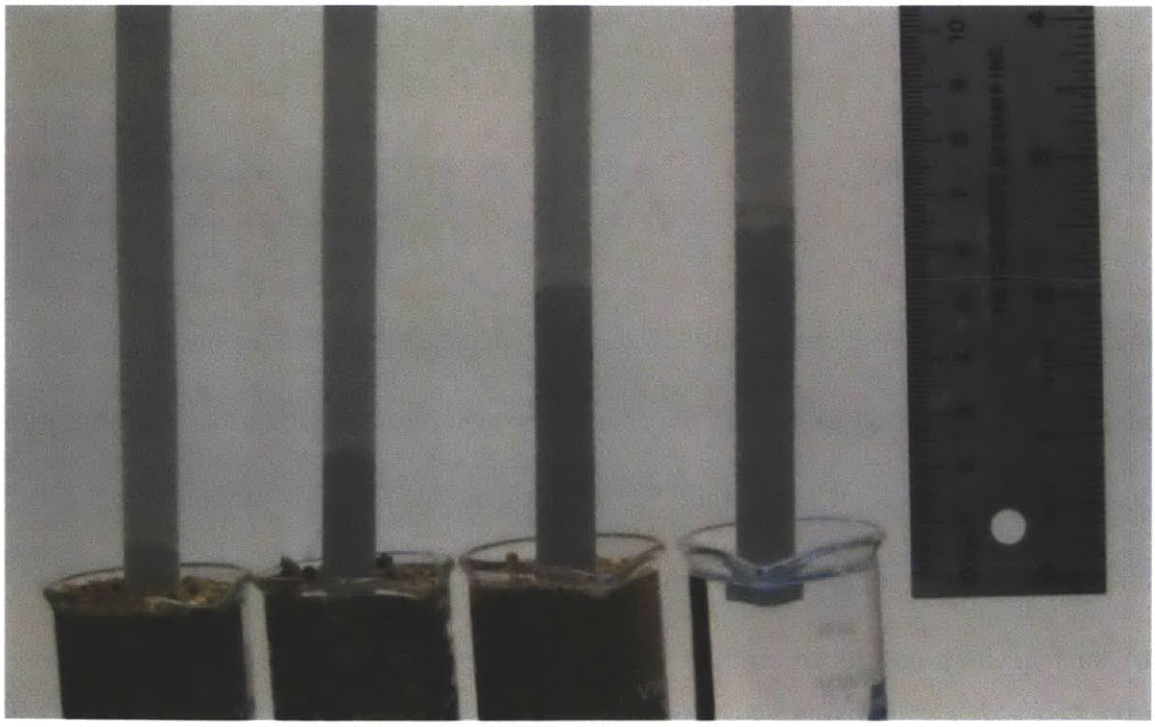

Figure 4-6: Soil capillary rise experiment result after 30 minutes. From left to right 5ml, 10ml, 11.5ml water was added into 35ml soil.

Chapter 5

Applications

5.1 Electrospray

Traditional electrospray uses stainless steel syringe tips, composite materials and even paper. According to each tips characteristics, the electrospray resulted in various droplet sizes. Using the BDA surface, we could expect that the electrospray would separate the solutes due to its chromatographic effect. The BDA surface also results in smaller droplets at the tip because BDA has smaller

pore size than the conventional electrospray. For electrospray using the BDA surface, we first determined the chromatographic effect, which can be used to separate the chemicals in solution according to their mobility. Electrospray properties were analyzed afterwards.

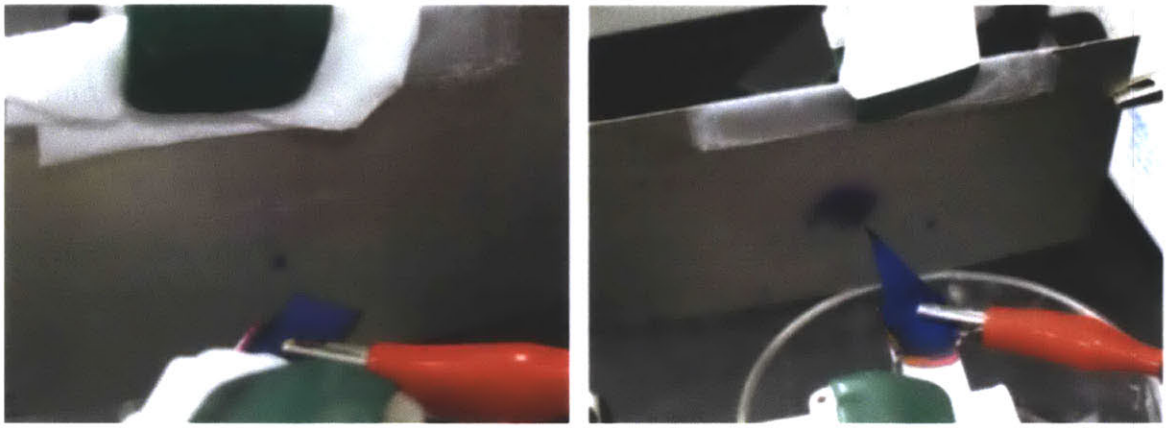

Figure 5-1: Electrospray performance comparison with respect to tip sharpness (angle of edge, left: 90°, right: 30°). Two pictures are taken after 10 seconds after power was applied.

5.1.1 Chromatography

We used a permanent marker (Sharpie) and an ethanol solution of fluorescein, rhodamine b, and methyl blue. The BDA surface was compared with the commercial TLC plate for their capability of chromatography. For the black

permanent marker, it separated yellow and green color by 70 mm from black ink while the commercial TLC plate only seperated the purple color 33mm. TLC plate failed to separate the yellow and green colors from the purple solute and stayed as a mixture at the maximum rise height 33 of mm.

Also when separating the rodamine b, methyl blue, and fluorescein 1.5 wt% methanol solution, TLC plates only separated red (Rodamine B), yellow (Fluorescein), and blue color (Methyl Blue) by 35mm, 37mm, and 40mm, respectively. The BDA surface moved the blue, yellow, and red color 5mm, 45mm, and 55mm, respectively. This verifies that the BDA surface showed better performance in terms of solute separation.

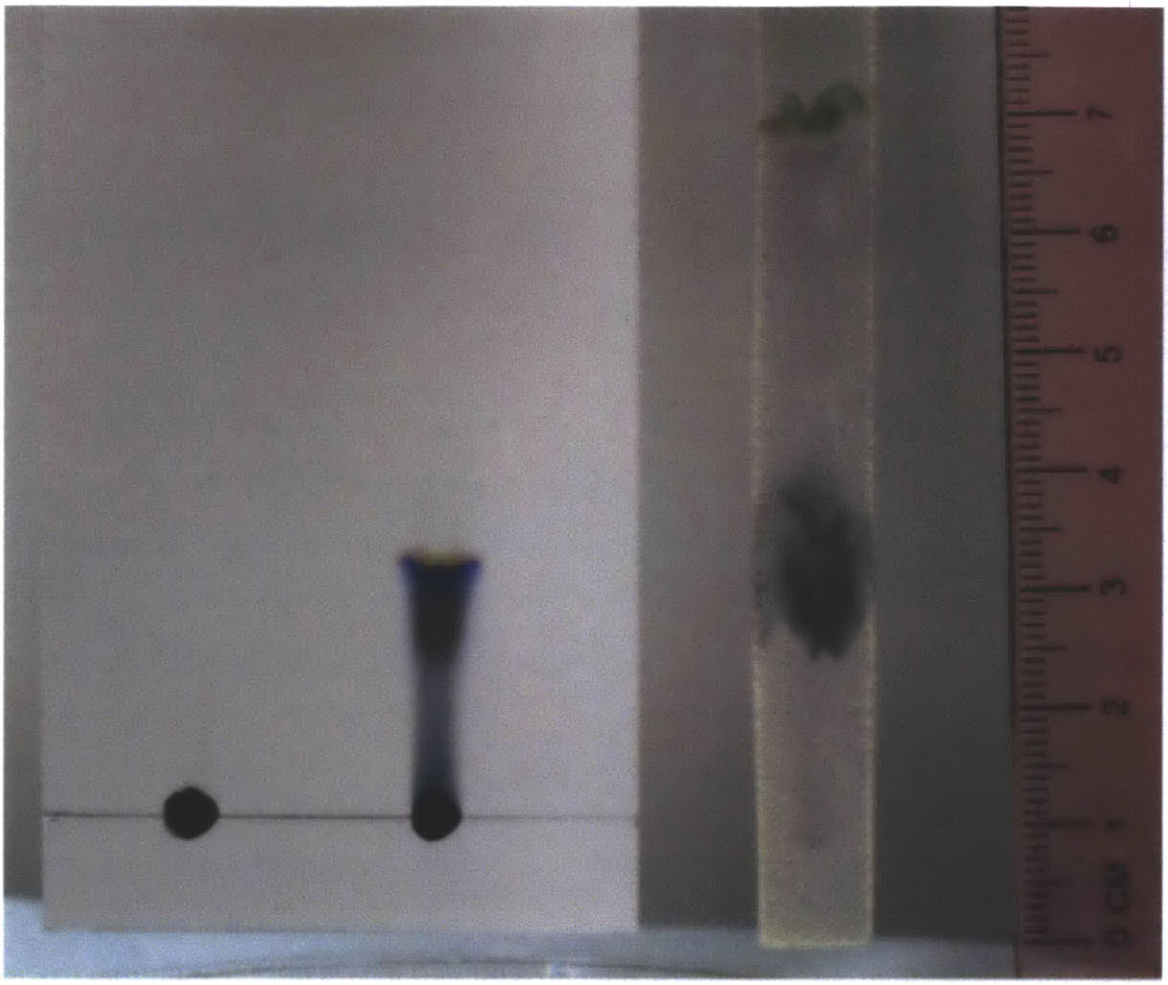

Figure 5-2: Chromatography performance comparison using black permanent ink on the TLC plate and the BDA surface.

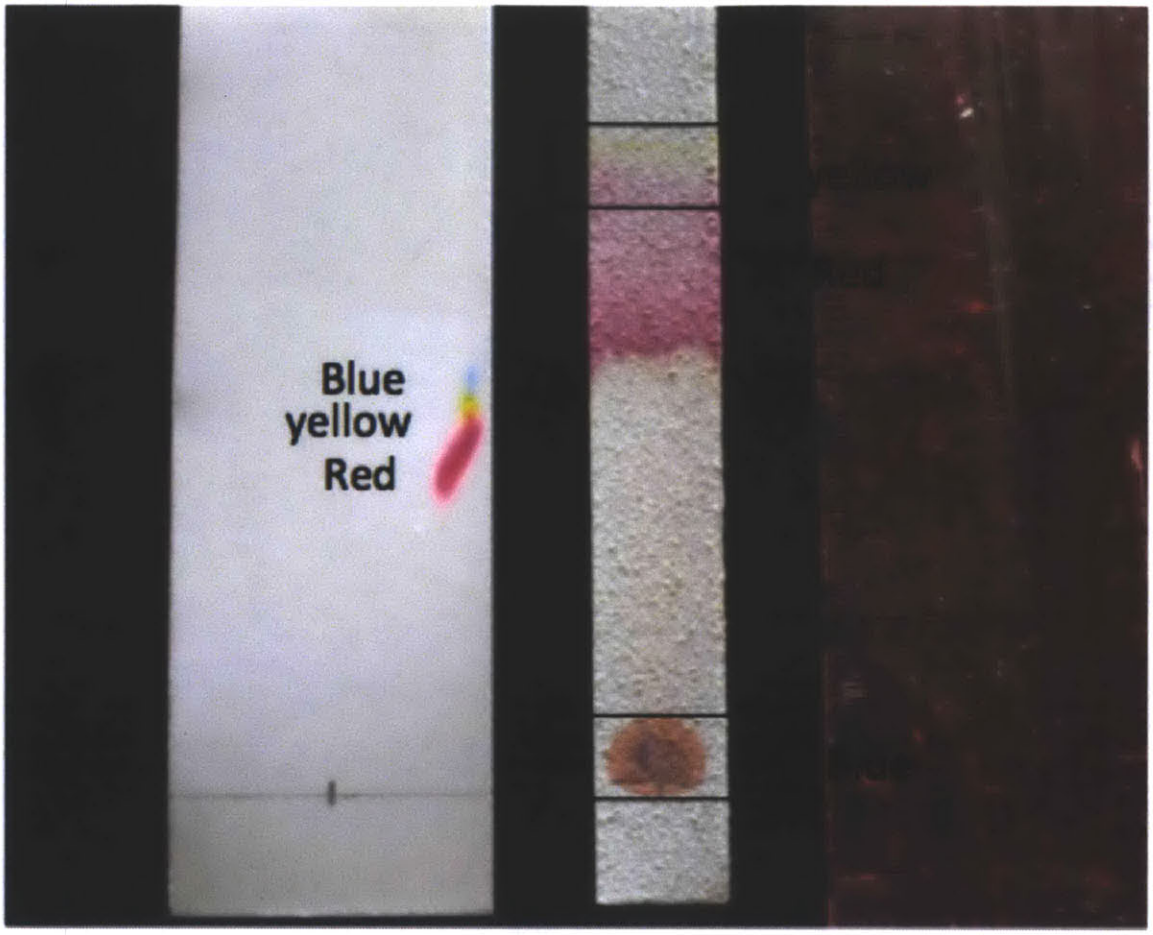

Figure 5-3: Chromatography performance comparison using Rodamine B, Methyle Blue, and Fluorescein 1.5 wt% Methanol solution on the TLC plate and the BDA surface.

5.1.2 Droplet Formation

A high speed camera (Ektapro model 1012, Redlake MASD Inc) was used to observe the formation of droplets at the tip of BDA surface.

<Taylor Cone Formation>

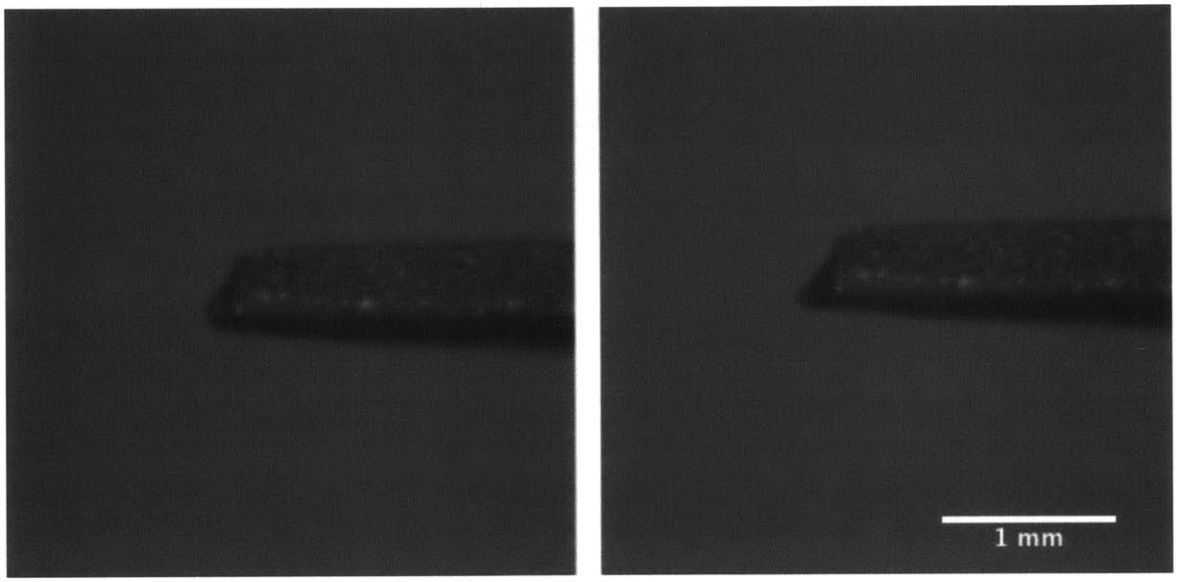

Figure 5-4: Left image was taken before establishing the Taylor cone. The right image was captured after 4 milliseconds.

Taylor cone formed at the tip of the BDA surface. The electric field pulls the solution to the left, overcoming the surface tension of the solution.

<Droplet Formation>

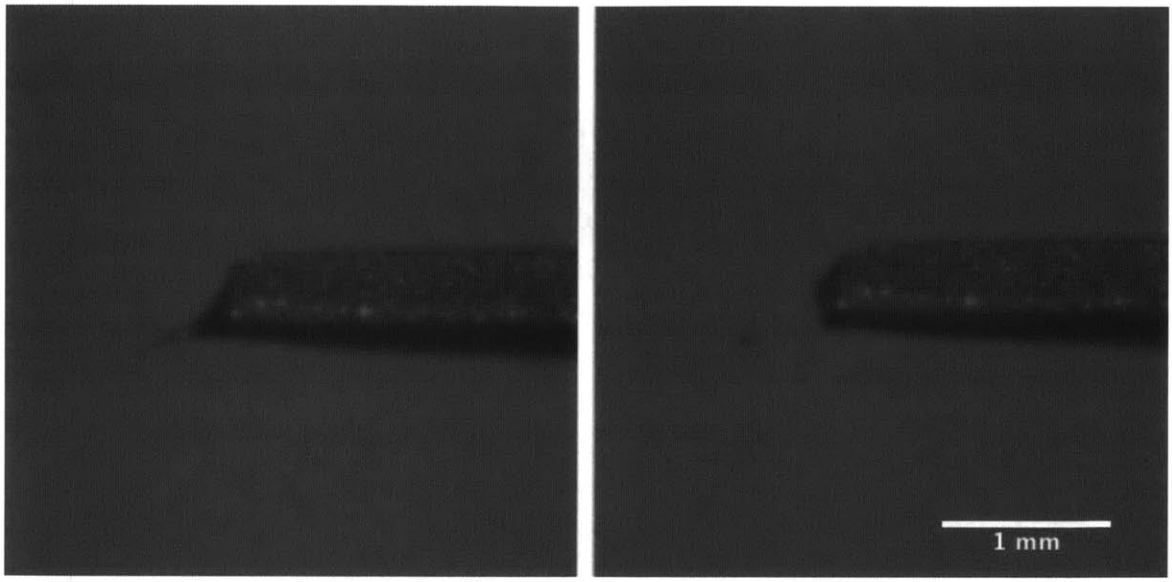

Figure 5-5: Droplet formation. After 4.3 ms of reference time and right is after 4.8 ms from reference time.

Droplets formed as the force from the electric field overcomes the surface tension of the liquid. When the electric field reaches the critical value, the liquid is stretched by the opposing electrical force and surface tension. Eventually the droplet totally separates from the liquid, yielding a spherical droplet.

<Droplet Average Speed>

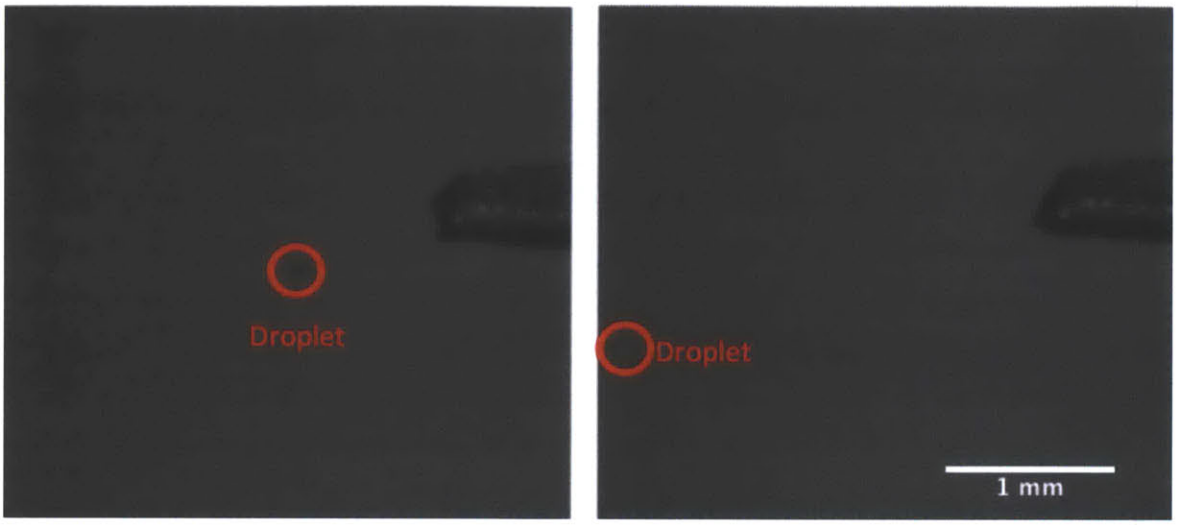

Figure 5-6: Droplet moving at the initial locations. Left is after 5.2 ms from the reference time, and 6.4 ms from the reference time.

In figure 5-6, droplet moved 1.7mm for 1.2 ms and the average droplet speed was 1.4m/s.

5.2 Hierarchical Structure by Etching Process

The BDA surface consists of irregular microstructures. These irregular micro structures contribute to its hydrophilicity. Adding nanoscale structures to the microstructures resulting from BDA would increase the surface area. The use of acid halide electrolyte such as HCl, and HF instead of using mild acid results in surface etching of titanium substrate.

As a result, homogeneous nano halls, which diameters are approximately 20nm, are successfully produced on the micro-porous structures of BDA surfaces. The hierarchical structures composed of micro and nano structures produced by BDA and etching provides much higher surface area than nanostructures of planar titanium surface. Moreover, using HCl as the electrolyte, instead of using the traditional electrolyte, HF, it could be fabricated in a safe environment.

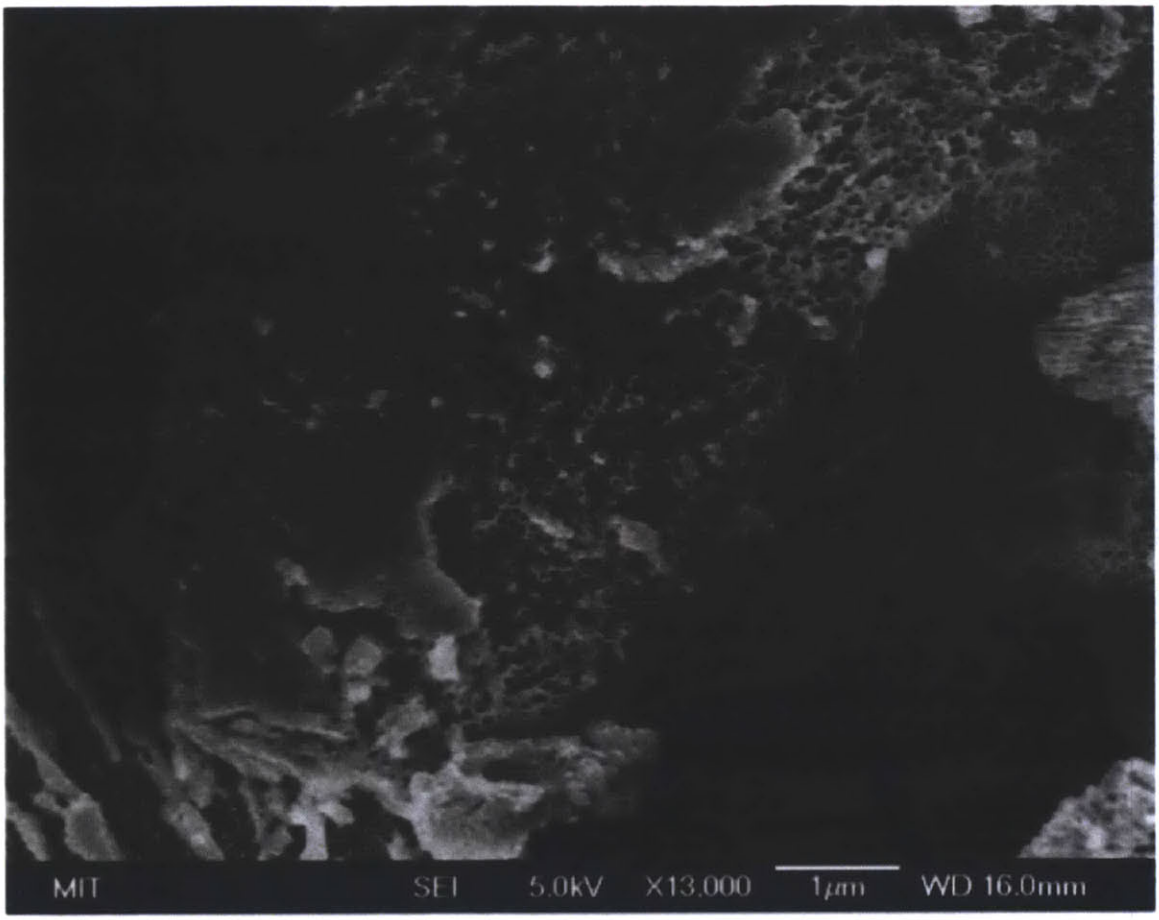

Figure 5-7: SEM image of hierarchical structure at micro scale. HCl was used as an electrolyte for etching process. Nano-structures are observed on micro-structures.

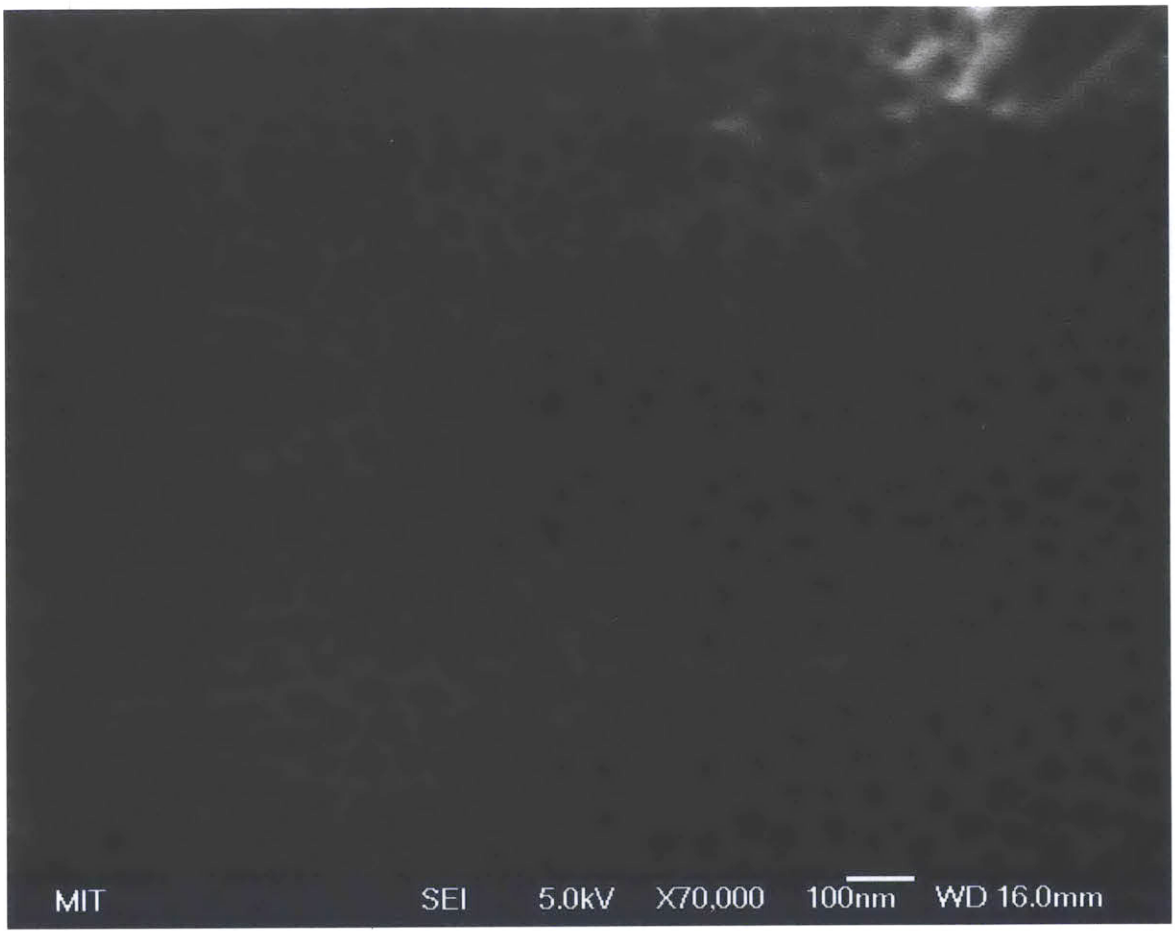

Figure 5-8: Nano Structures of Hierarchical Structure at High magnitude and can verify the nanostructures (approximate diameter: 20nm) on the micro-structures.

Chapter 6

Conclusions, and Future Work

We confirmed that BDA surfaces have better performance in terms of capillary pressure and spreading speed constant than that of commercial TLC plates. Also we found that we can adjust the BDA surface properties according to the fabrication conditions.

For the future work, mass spectrometry analysis is necessary to verify if the electrospray made by BDA surface successfully separates solutes from solution. Experiments were performed to maximize the droplet size and to verify that electrospray with the naked eye. Future work focuses more on minimize the droplet size for better analysis of solute by mass spectrometry.

Finally, more investigation in the hierarchical BDA surface is needed to obtain the enhanced surface areas to apply specific applications.

Bibliography

[1] Akira Fujishima, Kenichi Honda. "Electrochemical Photolysis of Water at a Semiconductor Electrode." *Nature*, no. 238 (1972): 37-38.

[2] M. Valden, X. Lai, D. W. Goodman. "Onset of Catalytic Activity of Gold Clusters on Titania with the Appearance of Nonmetallic Properties." *Science*, no. 281 (1998): 1647-1650.

[3] Brian O'Regan, Michael Gratzel. "A low-cost, high-efficiency solar cell based on dye-sensitized colloidal TiO2 films." *Nature*, no. 353 (1991): 737-739.

[4] Young-Taeg Sul, Carina B. Johansson, Sarunas Petronis, Anatol Krozer, Yongsoo Jeong, Ann Wennerberg, Tomas Albrektsson. "Characteristics of the surface oxides on turned and electrochemically oxidized pure titanium implants up to dielectric breakdown: the oxide thickness, micropore configurations, surface roughness, crystal structure and chemical composition ." *Biomaterials*, no. 23 (2002): 491-501.

[5] Washburn, Edward W. "The Dynamics of Capillar Flow." *The Physics Review* 17, no. 3 (1921): 273-283.

[6] Young Soo Joung and Cullen R. Buie "A Hybrid Method Employing Breakdown Anodization and Electrophoretic Deposition for

Superhydrophilic Surfaces ." *The Journal of Physical Chemistry B*, no. 117 (2013).

[7] J.M. Macak, H. Tsuchiya, A. Ghicov, K. Yasuda, R. Hahn, S. Bauer, and P. Schmuki. "TiO2 nanotubes: Self-organized electrochemical formation, properties and applications ." *Current Opinion in Solid State and Materials Science*, no. 11 (2007): 3-18.

[8] Neide K. Kuromoto, Renata A. Simão, and Gloria A. Soares. "Titanium oxide films produced on commercially pure titanium by anodic oxidation with different voltages ." *Maerials Characterization*, no. 58 (2007).

[9] Hiroaki Tsuchiya and Patrik Schmuki. "Thick self-organized porous zirconium oxide formed in H2SO4/NH4F electrolytes ." *Electrochemistry Communications*, no. 6 (2004): 1131-1134.

[10] I. Sieber, B. Kannan, and P. Schmuki. "Self-Assembled Porous Tantalum Oxide Prepared in H 2 SO 4 / HF Electrolytes." *Electrochemical and Solid-State Letters*, no. 8 (2005): J10-J12.

[11] Hiroaki Tsuchiya, Jan M. Macak, Irina Sieber, Luciano Taveira, Andrei Ghicov, Kamila Sirotna, and Patrik Schmuki. "Self-organized porous WO3 formed in NaF electrolytes." *Electrochemistry Communications*, no. 7 (2005): 295-298.

[12] Sato, N. "A Theory for Breakdown of Anodic Oxide Films on Metals." *Electrocimica Acta* 16 (1971): 1683-1692.

[13] M.W. Breiter, "Galvanostatic studies of passivity and breakdown of passivity of titanium in hydrochloric acid solutions." *Electrochimica Acta* 15, no. 7 (1970): 1195-1200.

[14] J. O'M. Bockris and E. C. Potter "The Mechanism of Hydrogen Evolution at Nickel Cathodes in Aqueous Solutions ." *The Journal of Chemical Physics* 20, no. 614 (1954): 614-628.

[15] M. Th. van. Genuchten, "A Closed-form Equation for Predicting the Hydraulic Conductivity of Unsaturated Soils." *Soil Science Society of America Journal* 44, no. 5 (1979): 892-898.

[16] Shada H. Krishnapillai, and Nadarajah Ravichandran. "New Soil-Water Characteristic Curve and Its Performance in the Finite-Element Simulation of Unsaturated Soils ." *INTERNATIONAL JOURNAL OF GEOMECHANICS* 12, no. 3 (2012): 209-219.

[17] L. B. LQEB, A. F. KIP, and G. G. Hudson. "Pnlses in Negative Point-to-Plane Corona." *Physics Review* 60 (1941): 714-722.

[18] Kenzo Hiraoka, Kentaro Nishidate, Kunihiko Mori, Daiki Asakawa and Shigeo Suzuki. "Development of probe electrospray using a solid needle." *Rapid Communications in Mass Spectrometry* 21 (2007): 3139-3144.

[19] Jingyueh Jeng, Che-Hsin Lin, and Jentaie Shiea. "Electrospray from Nanostructured Tungsten Oxide Surfaces with Ultralow Sample Volume ." *Analytical Chemistry* 77, no. 24 (2005): 8170-8173.

[20] Bin Hu, Pui-Kin So, Zhong-Ping Yao. "Analytical Properties of Solid-substrate Electrospray Ionization Mass Spectrometry ." *Americal Society for Mass Spectrometry* 24 (2012): 57-65.

[21] He Wang, Jiangjiang Liu, R. Graham Cooks, and Zheng Ouyang. "Paper Spray for Direct Analysis of Complex Mixtures Using Mass Spectrometry ." *Angewandte Chemie International Edition* 49 (2010): 877-880.

[22] Nicholas E. Manicke, Qian Yang, He Wang, Sheran Oradu, Zheng Ouyang, R. Graham Cooks. "Assessment of paper spray ionization for quantitation of pharmaceuticals in blood spots ." *International Journal of Mass Spectrometry* 300: 123-129.

[23] Jiangjiang Liu, He Wang, Nicholas E. Manicke, Jin-Ming Lin, R. Graham Cooks, and Zheng Ouyang. "Development, Characterization, and Application of Paper Spray Ionization ." *American Chemical Society* 82 (2010): 2463-2471.

[24] Ryan D. Espy, Ariel R. Muliadi, Zheng Ouyang, R. Graham Cooks. "Spray mechanism in paper spray ionization ." *International Journal of Mass Spectrometry* 325-327 (2012): 167-171.

[25] Lee Chuin Chen, Kentaro Nishidate, Yuta Saito,Kunihiko Mori, Daiki Asakawa, Sen Takeda, Takeo Kubota, Hirokazu Hori, and Kenzo Hiraoka. "Characteristics of Probe Electrospray Generated from a Solid Needle." *Journal of Physcal Chemistry B* 112 (2008): 11164-11170

[26] Xiaobo Chen, Maria Schriver, Timothy Suen, Samuel S. Mao. "Fabrication of 10nm diameter TiO2 nanotube arrays by titanium anodization." *Thin Solid Films* 515 (2007): 8511-8514.